Validation of localised corrosion model using real time corrosion monitoring in a chemical plant

A. Anderko[1], N. Sridhar*[2], L. T. Yang[2], S. L. Grise[3], B. J. Saldanha[3] and M. H. Dorsey[3]

A mechanistic model was developed and applied to predict the localised corrosion of a number of alloys in a plant process stream. In order to validate the model, multi-electrode array sensors (MAS) made from type 316L stainless steel and from two Fe–Ni–Cr–Mo–W alloys, AL6XN and alloy C–276, were installed in a side loop of a process stream in the chemical plant. The pitting corrosion rates measured from the probes were consistent with the plant equipment experience. The pitting rates obtained from the long term measurements were in good agreement with the actual corrosion rates obtained from post-test surface examination of the probes. The model successfully predicted the relative ranking of the alloys in this process environment. The pitting rates measured by the probes were consistent with model predictions.

Keywords: Chemical plant, Monitoring, Localised corrosion, Model, Stainless steel, Nickel base alloys, Sensor

Introduction

Localised corrosion is an important limiting factor in the performance of equipment used in the chemical process and other industries. However, predicting the occurrence of localised corrosion in chemical process streams has been largely based on empirical approaches. Standard laboratory tests in oxidising chloride solutions, such as ferric chloride, have yielded correlations between an alloy's localised corrosion resistance (e.g. critical pitting temperature) and its composition, expressed in terms of a 'pitting resistance equivalent' (PRE). However, the relative ranking of alloys in a standard laboratory solution does not always match that in a given process environment. If the laboratory solution is much more aggressive than the process environment, the tests may not differentiate between some of the lower alloys because all of them will suffer severe localised corrosion in the laboratory solution. In such a case, standard laboratory tests may eliminate potentially useful alloys for a given process. On the other hand, if the laboratory solution is much less aggressive than the process environment, it may not differentiate the high alloys because all of them will be resistant to localised corrosion. In such a case, the standard laboratory test may accept some alloys that are not sufficiently resistant.

Tests conducted in simulated process environments along with prior experience in related processes provide an important improvement over tests using standard laboratory solutions. However, it is expensive to test all the variations that occur in a real process stream. Pilot plant studies of new processes can also provide insights into materials selection. However, a reduced timeframe for implementing process changes or bringing new products to market often precludes detailed experimental studies. Therefore, predicting the performance of materials in process environments without process specific corrosion tests can lead to significant cost savings to the industry. Furthermore, narrowing the list of alloys for testing through 'computer experiments' enables in depth laboratory studies of the effects of process parameters on corrosion.

Considerable progress has been made in the last three decades in understanding the initiation, growth, and repassivation of localised corrosion of many metallic materials, as reflected in several conference proceedings and books.[1–6] Modelling the localised corrosion process has been performed considering atomic/molecular processes,[7,8] microstructural features,[1,9] and transport processes.[10–13] While these models have successfully explained different aspects of pitting and crevice corrosion, they have not been used as predictive tools in plant applications. The atomistic/molecular models require too many parameters that cannot be readily measured. The crevice transport models involve geometrical factors that cannot be easily measured for complex process equipment as these surfaces have many different gaps.[14]

A different approach to predicting localised corrosion in complex chemical environments typically encountered in the chemical process industry was proposed in a previous paper.[15] The approach essentially divides the

[1]OLI Systems, Inc., 108 American Way, Morris Plains, NJ 07950, USA
[2]Southwest Research Institute, 6220 Culebra Road, San Antonio, TX 78228, USA
[3]DuPont Engineering, PO Box 80323, Wilmington, DE 19880-0323, USA

*Correponding author, email nsridhar@swri.org

Published by Maney on behalf of the Institute
Received 17 November 2004; accepted 14 January 2005
DOI 10.1179/174327805X29840

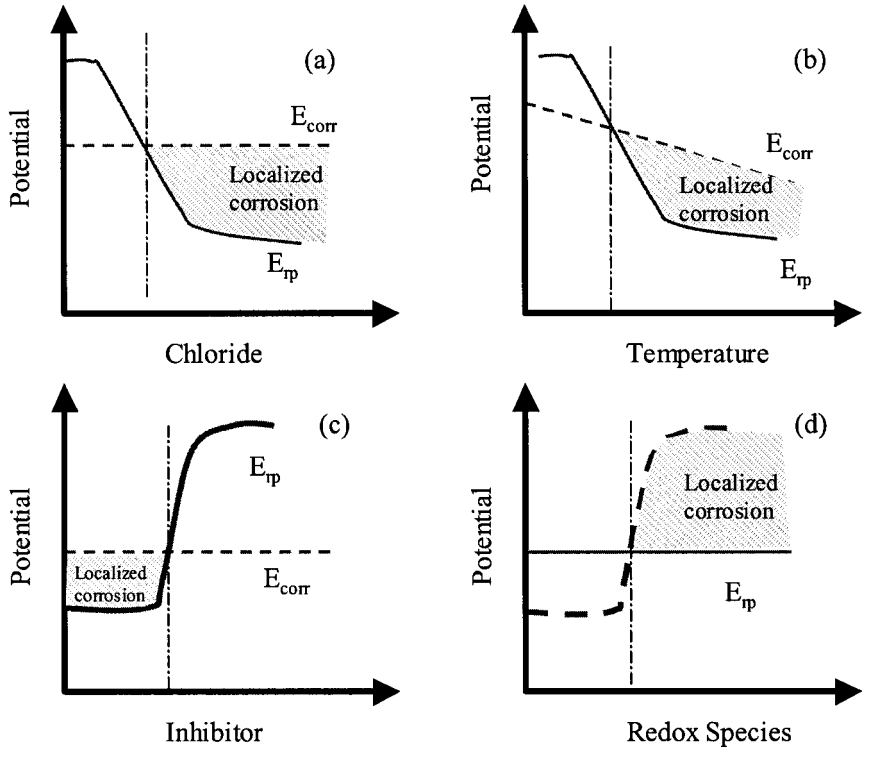

1 Schematic illustration of comparison of repassivation and corrosion potentials E_{rp} and E_{corr} for different environmental parameters. Shaded areas denote localised corrosion

task of predicting localised corrosion into two independent parts: predicting the repassivation potential for localised corrosion and the corrosion potential. The repassivation potential E_{rp} is a measure of the tendency of an alloy to suffer localised corrosion in an environment. The underlying justification for the use of E_{rp} is the fact that for engineering applications, only the fate of stable pits or crevice corrosion is important. Pits that nucleate, but do not grow beyond an embryonic stage (metastable pits) do not adversely affect the performance of engineering structures. It has been shown in previous publications[15–17] that (i) the E_{rp} is the potential below which stable pitting or crevice corrosion does not occur and (ii) it is relatively insensitive to prior pit depth and surface finish. The predicted repassivation potential is then compared to the corrosion potential E_{corr} in the same environment to determine the alloy's susceptibility to localised corrosion. The separation of the problem into two parts involving E_{rp} and E_{corr} is valid because E_{corr} is not affected by localised corrosion at the early stages where the area of the actively corroding pit is insignificant compared to the overall area.

The concept is illustrated schematically in Fig. 1. For a given alloy, the repassivation potential E_{rp}, also called the protection potential, decreases with an increase in chloride concentration. In the general case, three or more regions in the E_{rp} may be observed,[15,17] but in some cases only a semilogarithmic decrease may be observed. The corrosion potential is not a strong function of chloride concentration, unless significant localised corrosion occurs, because in the absence of localised corrosion the passive current density is not strongly dependent on chloride concentration.[2] The critical chloride condition for localised corrosion to occur is when E_{rp} is lower than E_{corr} (Fig. 1*a*). Similarly, for a given chloride concentration a critical temperature (Fig. 1*b*) and a critical inhibitor concentration exist (Fig. 1*c*). In many processes, incidental contamination of the process fluid by redox species may increase the E_{corr} such that localised corrosion may occur beyond a critical concentration of redox species. The actual condition in a system may be a combination of the idealised cases shown in Fig. 1*a–d*. In a previous paper,[15] a model was developed to calculate the repassivation potential of alloys in environments containing aggressive, non-aggressive and inhibitive ions. This model has been validated for a number of alloys from the Fe–Ni–Cr–Mo–W family.

The application of this approach to a plant process stream is discussed in this paper. Multi-electrode array sensors (MAS) were installed in the side loop of the plant process to determine the localised corrosion susceptibility of various alloys. Along with the MAS probes, external pressure balanced, Ag/AgCl reference electrodes were installed to track E_{corr} of both the MAS electrodes and the process piping material. The present paper compares the model predictions to sensor measurements.

Computational model

Repassivation potential calculations

The repassivation potential model[15] considers the electrochemistry of a metal M that undergoes dissolution underneath a layer of concentrated metal halide solution MX. The concentrated solution may or may not be saturated with respect to a hydrous solid metal halide. The thickness of the hydrous halide layer is assumed to be much smaller than the size of the pit so that the system may be regarded as one dimensional. In

the process of repassivation, a thin layer of oxide forms at the interface between the metal and the hydrous metal halide. The model assumes that, at a given instant, the oxide layer covers a certain fraction of the metal surface. This fraction increases as repassivation is approached. Further, the model includes the effects of multiple aggressive and non-aggressive or inhibitive species, which are taken into account through a competitive adsorption scheme. The aggressive species form metal complexes, which dissolve in the active state. On the other hand, the inhibitive species and water contribute to the formation of oxides, which induce passivity. In general, the equations that describe these processes are complex and can be solved only numerically. However, a closed-form equation has been found in the limit of repassivation, i.e. when the current density reaches a predetermined low value i_{rp} (typically $i_{rp}=10^{-2}$ A m^{-2}) and the fluxes of metal ion become small and comparable to those for passive dissolution. This closed form expression, which can be solved to calculate the repassivation potential, is given by

$$1+\sum_{i}\left[\left(\frac{i_{rp}}{i_p}-1\right)\frac{l_i''}{i_{rp}}\right]\theta_j^{n_j}\exp\left(\frac{\xi_i F E_{rp}}{RT}\right)=\sum_{j}\frac{k_j''}{i_{rp}}\theta_j^{n_j}\exp\left(\frac{\alpha_j F E_{rp}}{RT}\right) \quad (1)$$

where E_{rp} is the repassivation potential, i_p is the passive current density, T is the temperature, R is the gas constant, and F is the Faraday constant. In equation (1) k_j'' is the rate constant for the reaction mediated by the adsorption of aggressive species j; l_i'' is the rate constant for the reaction mediated by the adsorption of an inhibitive species i; nj is the reaction order with respect to species j; and α_j and ξ_i are the transfer coefficients of the aggressive and inhibitive species, respectively. The partial coverage fraction θ of a species j is related to the activity of this species in the bulk solution by

$$\theta_j=\frac{r_j a_j}{1+\sum_k r_k a_k} \quad (2)$$

Equation (1) contains the following parameters:

(i) Scaled rate constant for aggressive ions, which can be expressed using a scaled Gibbs energy of activation $\Delta g_{A,j}^{\neq}$:

$$k_j=\frac{k_j}{i_{rp}}=\exp\left(-\frac{\Delta g_{A,j}^{\neq}}{RT}\right) \quad (3)$$

(ii) Scaled rate constant for inhibitive species, which is also expressed using a scaled Gibbs energy of activation $\Delta g_{I,i}^{\neq}$:

$$\left(\frac{i_{rp}}{i_p}-1\right)\frac{l_i''}{c}=\exp\left(-\frac{\Delta g_{I,i}^{\neq}}{RT}\right) \quad (4)$$

(iii) Reaction order with respect to aggressive ions nj, which is used in equation (1) in conjunction with the coverage fraction θj.

(iv) Electrochemical transfer coefficients for the inhibitive species ξi.

(v) Scaled Gibbs energy of adsorption $\Delta G_{ads,i}$, which defines the adsorption coefficient in equation (2):

$$r_j=\exp\left(-\frac{\Delta G_{ads,j}}{RT}\right) \quad (5)$$

However, the latter property can be assigned a common default value for most species. This is a simplification that is made in order to reduce the number of independent adjustable parameters in the model. Although it would be possible to determine this quantity from independent measurements, it is more practical to determine a minimum set of adjustable parameters using only repassivation potential data. Although the value of the Gibbs energy of adsorption affects the values of the Gibbs energies of activation for aggressive (equation 3) and inhibitive (equation 4) species, very similar agreement with experimental data can be obtained using Gibbs energies of adsorption that fall within a certain range (from 5 to 15 kJ mol^{-1}) for most species. Therefore, the assumption of a default value of $\Delta G_{ads,i}$ does not have a detrimental effect on the accuracy of calculations for most species. The differences in the localised corrosion properties of various species are then sufficiently accounted for by the differences in the values of the Gibbs energies of activation $\Delta g_{A,j}^{\neq}$ and $\Delta g_{I,i}^{\neq}$. However, this rule does not apply to very strongly inhibitive species such as nitrates, for which it is necessary to adopt a species specific value of $\Delta G_{ads,i}$.

The scaled Gibbs energies of activation (equations (3) and (4)) for aggressive and inhibitive species may be further related to temperature by

$$\frac{\Delta g_{A,j}^{\neq}}{T}=\frac{\Delta g_{A,j}^{\neq}(T_{ref})}{T_{ref}}+\Delta h_{A,j}^{\neq}\left(\frac{1}{T}-\frac{1}{T_{ref}}\right) \quad (6)$$

and:

$$\frac{\Delta g_{I,i}^{\neq}}{T}=\frac{\Delta g_{I,i}^{\neq}(T_{ref})}{T_{ref}}+\Delta h_{I,i}^{\neq}\left(\frac{1}{T}-\frac{1}{T_{ref}}\right) \quad (7)$$

Further, the electrochemical transfer coefficients for aggressive species α_j are assumed to be equal to one and the reaction orders for the effects of inhibiting species nj can be assigned a default value of one. These parameters can be assigned default values because the accuracy of representing experimental repassivation potential data is not sensitive to their values, as long as they remain within a $\pm 50\%$ range. At the same time, the use of default parameters reduces the number of adjustable parameters that have to be determined from experimental data.

The parameters of the model and their physical meaning are summarised in Table 1 for the main species that are of interest in this study. The parameters for H_2O and Cl- have been regressed to match experimental repassivation potential data in aqueous chloride solutions at various chloride concentrations and temperatures. The parameters for OH- have been obtained using E_{rp} data in mixed Cl- + OH- solutions. The procedure for determining the parameters was described in the previous paper for metals in aqueous solutions containing aggressive, non-aggressive and inhibitive species.[15]

As described above, the repassivation potential model has a limiting character, i.e. it accurately represents the

Table 1 Parameters of repassivation potential model for type 316L stainless steel, alloy AL6XN, and alloy C–276 in contact with the primary species in system studied

Parameter	Physical meaning	Alloy	Values for selected species				Units
			H2O	Cl-	OH-	CO32-	
$\Delta g^{\neq}_{A,j}(T_{ref})$	Gibbs energy of activation for dissolution reaction mediated by adsorption of aggressive species at reference T (298·15 K)	316L AL6XN C–276	not applicable	−10·92 12·19 19·85	not applicable	not applicable	kJ mol^{-1}
$\Delta h^{\neq}_{A,j}$	Enthalpy of activation for dissolution reaction mediated by adsorption of aggressive species	316L AL6XN C–276	not applicable	0·040 0·102 0·091	not applicable	not applicable	kJ mol^{-1}
$n_{A,j}$	Reaction order with respect to aggressive ions	316L AL6XN C–276	not applicable	1·46 1·3 1·6	not applicable	not applicable	
$\Delta g^{\neq}_{I,j}(T_{ref})$	Gibbs energy of activation for the formation of oxide mediated by the adsorption of inhibitive species at reference T	316L AL6XN C–276	19·31 35·76 24·76	not applicable	−7·15 not determined not determined	not determined	kJ mol^{-1}
$\Delta h^{\neq}_{I,j}$	Enthalpy of activation for the formation of oxide mediated by the adsorption of inhibitive species	316L AL6XN C–276	0* 0·089 0·013	not applicable	0** not determined not determined	not determined	kJ mol^{-1}
ξ_{Ij}	Electrochemical transfer coefficient for inhibitive species	316L AL6XN C–276	0·743 0·9** 0·9**	not applicable	0·99 not determined not determined	not determined	
$\Delta G_{ads,j}$	Gibbs energy of adsorption	All alloys	10**	10**	10**	10**	kJ mol^{-1}

* The value 0 indicates that the temperature dependence of the Gibbs energy of activation is insignificant.
** Default value, not adjusted using experimental data.

state of the system in the repassivation potential limit. In addition to the value of the repassivation potential, the model predicts the correct limiting slope of the current density versus potential relationship as the potential deviates from E_{rp}.[15] As discussed in a previous paper,[15] the predicted slope is accurate in the limit of repassivation (i.e. for $E \rightarrow E_{rp}$). As the potential increasingly deviates from E_{rp}, the predicted current density becomes progressively larger than the experimental values. In such cases, the model provides an upper estimate for the current density for the propagation of individual pits. The current density predicted by the model as a function of potential is given by

$$i = \frac{\sum_j k_j'' \theta_j^{n_j} \exp\left(\frac{\alpha_j FE}{RT}\right) + \sum_i l_i'' \theta_i^{n_i} \exp\left(\frac{\xi_i FE}{RT}\right)}{1 + \frac{1}{i_p}\sum_i l_i'' \theta_i^{n_i} \exp\left(\frac{\xi_i FE}{RT}\right)} \quad (8)$$

Equation (8) reduces to equation (1) for $E=E_{rp}$ and $i=i_{rp}$. Since equation (8) is a limiting law, its accuracy gradually deteriorates as the potential increasingly deviates from E_{rp}. Equation (8) cannot be regarded as a complete model for the propagation rate of an actively growing pit because it does not take into account factors such as the ohmic potential drop, diffusion limitations, etc. However, the current density predicted using equation (8) for $E>E_{rp}$ is useful because it provides an estimate of the maximum propagation rate of an isolated pit as a function of potential. Such an upper estimate is particularly convenient because it relies only on parameters that have been calibrated using repassivation potential data.

Corrosion potentials

The starting point for the corrosion potential[18,19] model is the computation of speciation in the investigated system. For this purpose, a thermodynamic model is used to predict the concentrations and activities of both ionic and neutral species in multi-component systems that may contain an aqueous phase, any number of solid phases and, if necessary, a vapour and a non-aqueous liquid phase. The activities of individual species are further used in the electrochemical model. After completing speciation calculations, diffusion coefficients of individual species and the viscosity of the solution are computed using separate models.[20,21] The electrochemical model[18,19] takes into account reactions on the surface of the metal and transport processes for the species that participate in the reactions. The model includes passivation phenomena, which may be influenced by pH and the presence of aggressive or inhibitive species in the solution. In this study, it was known that some of these redox species arising from catalysts and other process components could contribute significantly to the corrosion potential. However, since their concentrations were not known, reliance was placed on the measured corrosion potentials.

Laboratory and plant studies

Laboratory measurements of E_{rp} and E_{corr} were conducted in both laboratory solutions and fluids obtained from the plant process stream. The procedures for measurements of these potentials are given in the previous paper.[15] Concurrently with laboratory studies, real time monitoring tests were conducted in a plant process stream using coupled multi-electrode array sensors to validate the model.[22] The monitored process stream consisted of a nearly saturated chloride brine. Minor impurities included iron (Fe), copper (Cu), nickel (Ni) and magnesium (Mg). None of the impurities exceeded a concentration of 10 mg L^{-1}. Nominal operating conditions involved a temperature of 100°C, pH ranging from 8 to 10, and a superficial liquid velocity of 0·61 m s^{-1} through the loop. Detailed results of the plant study have been presented elsewhere.[22]

Coupled multi-electrode array sensors

The principle of the coupled multi-electrode array sensor (MAS) has been described elsewhere.[23,24] In a MAS, multiple miniature electrodes are the active sensing element of the sensor. These miniature electrodes are made of metals identical to the material of construction of the process, and whose corrosion rate is of monitoring interest, and are coupled to a common joint through independent resistors. Thus, each electrode simulates or represents part of a corroding metal if the sensor is in a corrosive environment. In a localised corrosion environment, anodic currents flow into the more corroding electrode and cathodic currents flow out of the less or non-corroding electrodes. Such currents are measured from the voltages across the resistors and are used as the signals for localised corrosion.

Three MAS probes were used, each consisting of eight identical solution annealed wires of stainless steel 316L (UNS S31603), AL6XN (UNS N08367) and alloy C–276 (UNS N10276). The compositions of these alloys are shown in Table 2. The probes were designed[22] for applications at pressures as high as 10·88 MPa and temperatures as high as 230°C. The tubing material for all the probes was alloy C–276. The sensing electrodes were flush mounted in polytetrafluoroethylene (PTFE). The surface area of each electrode in the sensors was 0·00567 cm^2. Prior to the test, the sensing surfaces of the probes were polished with 600 grit paper and cleaned with acetone. A side loop was constructed out of alloy C–22 (UNS N06022) into which the MAS probes, linear polarisation resistance (LPR) probes, and a high temperature reference electrode were installed.[22] The reference electrode was an external pressure balanced Ag/AgCl electrode.[25] The LPR probes were for a different test and their results are not reported in this

Table 2 Chemical compositions (wt-%) of the alloys used in the sensors

Alloys	UNS #	Fe	Ni	Cr	Mo	Cu	W	C	Others
316L SS	S31603	Bal.	12	17·58	2·1	0·31		0·028	1·4 Mn
AL6XN	N08367	48·22	23·92	20·43	6·19	0·16	0·03	0·02	0·2 N
C-276	N10276	5·51	58·75	15·64	15·54	0·19	3·74	0·002	0·41 Mn 0·17 Co

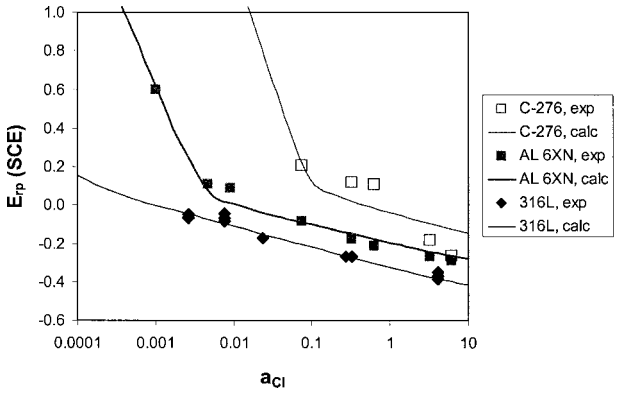

2 Calculated and experimental repassivation potentials for type 316L stainless steel and alloys AL6XN and C–276 at 95°C

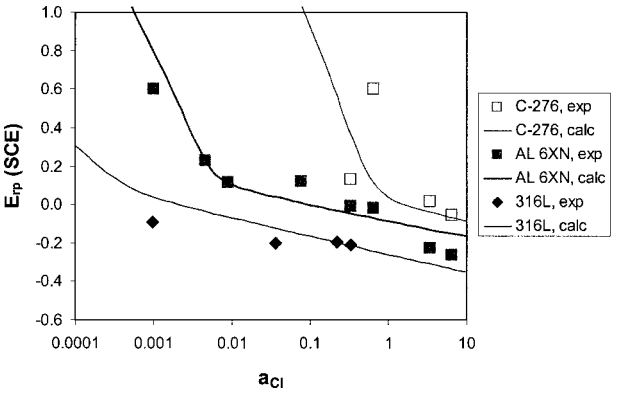

3 Calculated and experimental repassivation potentials for type 316L stainless steel and alloys AL6XN and C–276 at 60°C

paper. Data for the MAS probes and electrochemical potentials were collected via a fibreoptic cable in the plant digital control system and downloaded remotely.

Validation of the model

Laboratory solutions

In a previous paper,[15] the model has been shown to reproduce the results of experimental measurements of E_{rp} for selected alloys in contact with various combinations of aggressive, non-aggressive and inhibitive ions. Here, we apply the model to the three metals that were the subject of the plant tests (i.e. type 316L stainless steel, alloy AL6XN and alloy C–276) in well defined solutions containing the ions that are majority components in the process stream.

The primary corrosive component in the process brine is the chloride ion. Therefore, the model has been calibrated against experimental data in pure chloride solutions at temperatures ranging from 23°C to 150°C. The model parameters are summarised in Table 1. Figures 2 and 3 show the calculated and experimental repassivation potentials as functions of chloride activity at 95°C and 60°C, respectively. The temperature of the process stream is fairly close to 95°C whereas the 60°C isotherm illustrates the temperature dependence of the repassivation potential. The model reproduces the experimental data essentially within experimental uncertainty. In particular, the transition between the high slope and low slope portions of the $E_{rp}(a_{Cl})$ curve is accurately computed.

In addition to chlorides, carbonates and hydroxides are also significant components of the stream. In contrast to chlorides, carbonates and hydroxides do not induce localised corrosion and act as weak inhibitors. Figure 4 shows the dependence of E_{rp} on the activity of hydroxide ions for two concentrations of chloride ions (i.e. 0·5 and 4M). Up to a certain concentration of hydroxides, the E_{rp} curve is flat and shows a minimal dependence on alkalinity. Then, it increases rapidly at a critical hydroxide activity, which depends on the activity of chlorides. This transition corresponds to the inhibition of localised corrosion by hydroxides. Since hydroxides are only weak corrosion inhibitors, the activity of OH- that is necessary to increase the repassivation potential is relatively high. For example, concentrations of hydroxide ions of the order of several M are required to inhibit a system containing 4M Cl-. The same behaviour is shown by carbonate ions.

The investigated process stream is dominated by chloride ions and is relatively weakly alkaline. Therefore, the repassivation potential is expected to lie on the flat portion of the curve that depicts the dependence of E_{rp} on hydroxide or carbonate activity.

Model validation using laboratory tests of process fluids

Having calibrated the model using laboratory data for well defined simple systems, the next step was to apply it to complex plant streams. For this purpose, the composition of the plant fluid was determined on the basis of a laboratory analysis. The process stream is dominated by chlorides, with some carbonates, sulphates and numerous impurities. It should be noted that impurities are not likely to affect the repassivation potential unless they act as very strong corrosion inhibitors. For the purpose of simulation, it has been assumed that the stream contains 5·644M NaCl, 0·1336M Na_2CO_3, 0·0048M Na_2SO_4, 0·0019M Na_2SO_3, and 0·0386M HCl. HCl was used in the simulation to match the observed pH value of the stream. Calculations to match the pH value were

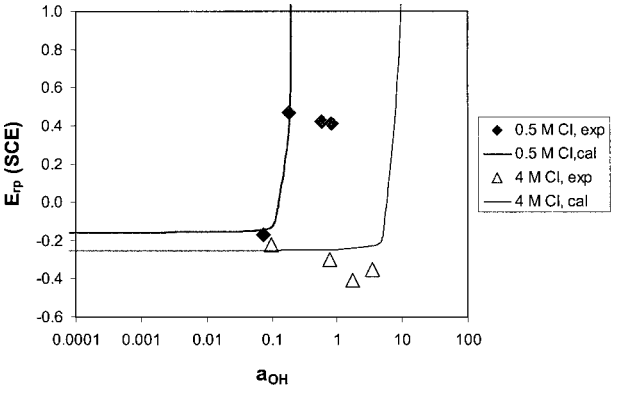

4 Combined effect of chloride and hydroxide ions on repassivation potential of type 316L stainless steel at 23°C. The experimental points above 0·6 V (SHE) correspond to transpassive dissolution and reflect the absence of localised corrosion

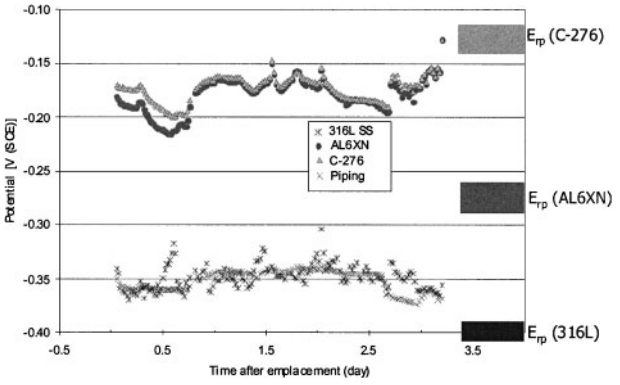

5 Comparison of experimental corrosion potential data with predicted repassivation potentials for short term plant corrosion tests. The calculated repassivation potentials are depicted by rectangles. The height of the rectangles reflects the uncertainty of temperatures, which are assumed to vary from 95°C to 105°C.

performed using the OLI thermodynamic model.[25] The temperature of the stream is close to boiling and the system is close to saturation.

In the first step, the repassivation potentials were calculated for the three alloys that were investigated in the process fluid. Since the exact temperature was unknown, the calculations were performed at 95 and 105°C. The results are shown in Table 3. The agreement for alloys C–276 and AL6XN is excellent as the deviations are smaller than experimental uncertainty (typically ± 100 mV). The agreement for type 316L stainless steel is not as good as for the other alloys, but is still reasonable. It should be noted that the process fluid data were not used to calibrate any model parameters. Thus, this test provided a very stringent test of the model and proved its accuracy.

Model validation using in process monitoring

In this step, the calculated repassivation potentials in plant process fluid were compared with the experimentally observed corrosion potentials for the three alloys. The experimental measurements of the corrosion potentials were made in the side stream of the process fluid using an Ag/AgCl reference electrode and then converted to the SHE scale. The results are shown in Figure 5 for short term measurements ($\sim$3 days) and in Fig. 6 for long term measurements ($\sim$6 weeks).

It should be noted that only the corrosion potentials for alloys C–276 and AL6XN in Figs 5 and 6 can be regarded as corrosion potentials established on a passive surface. They are essentially the same, which is to be expected for alloys from this family. Such corrosion potentials are obtained when the extent of localised corrosion is relatively small. The initiation of localised corrosion is controlled by these potentials. On the other hand, the measured corrosion potentials for type 316L stainless steel are affected by the progress of localised corrosion and are closer to the pitting potential than to the corrosion potential. They constitute effective corrosion potentials that are affected by electrochemical processes on both the passive surface and within the actively growing pits. The experimentally observed corrosion potentials fluctuate in fairly wide ranges because of varying concentrations of impurities, some of which are active redox species. Also, the substantial variations in the long term tests are partially related to scaling phenomena on the electrodes.

The difference between the corrosion and repassivation potentials is a measure of the tendency for localised corrosion. Accordingly, type 316L stainless steel is predicted to undergo rapid localised corrosion because the corrosion potential is much higher than the repassivation potential. A smaller, but significant tendency is predicted for AL6XN, which has an intermediate repassivation potential. In the case of alloy C–276, either no tendency or a small tendency for localised corrosion is observed depending on the value of the corrosion potential. In the plant tests,[22] rapid localised corrosion was observed for type 316L stainless steel and significantly lower corrosion was measured for AL6XN (Fig. 7). For alloy C–276, essentially no localised corrosion was observed (Fig. 7). Thus, it can be concluded that model predictions based on the repassivation potential are in good agreement with plant

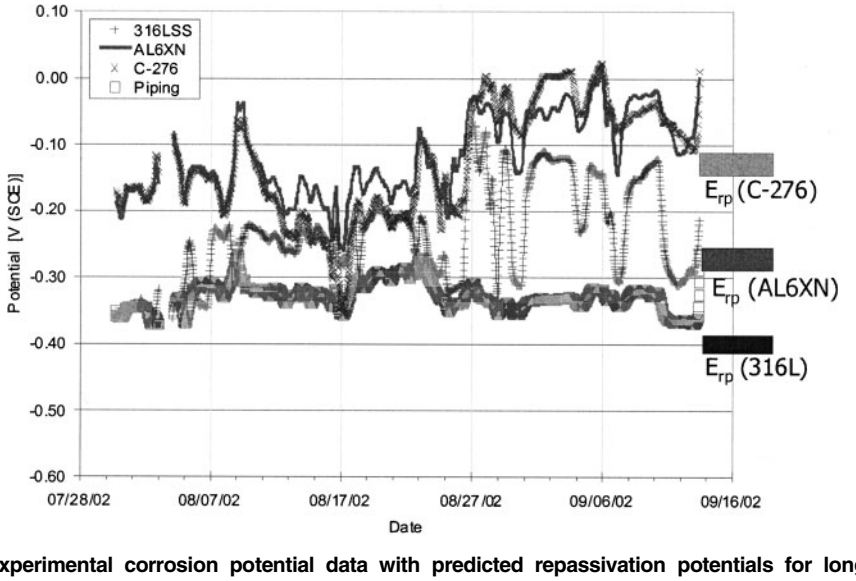

6 Comparison of experimental corrosion potential data with predicted repassivation potentials for long term plant corrosion tests. Calculated repassivation potentials are depicted by rectangles. The height of the rectangles reflects the uncertainty of temperatures, which are assumed to vary from 95°C to 105°C

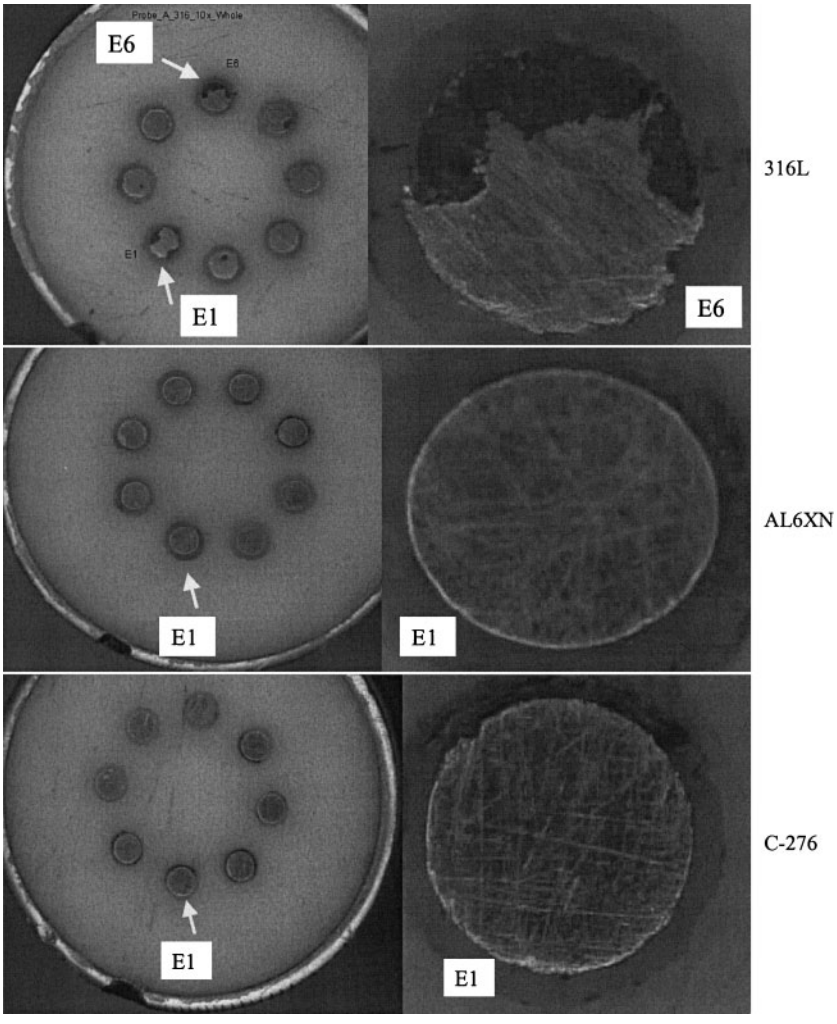

7 Sensing surfaces of three alloy probes after 45 day service in the side loop of hot brine stream

observations. The data from field test racks of these materials and the performance of process components made of these materials are also consistent with the long-term trend in the corrosion potentials.[27] These racks consisted of crevice coupons exposed to the plant process stream over different time periods. Type 316L stainless steel showed deep crevice corrosion and some evidence of stress corrosion cracking. AL6XN showed moderate crevice corrosion. alloy C–276 showed slight crevice corrosion in one of the coupons.

Finally, it must be noted that in both Figs 5 and 6, the plant piping material, made of alloy,[22] showed a much lower corrosion potential than the C–276 and AL6XN electrodes. This may be because of galvanic effects between the alloy[22] piping and other process components made of stainless steel and other more active materials. The electrodes were isolated from the piping material and therefore would not be influenced by other process components. The performance of the piping material was not monitored during this project.

In the final step of the analysis, equation (8) has been used to estimate the maximum propagation rate of individual pits. The propagation rate calculated from equation (8) is shown in Fig. 8 for the three alloys as a function of the potential at two temperatures (95°C and 105°C). As discussed in a previous paper,[15] the predicted current density versus potential relationships for the propagation of individual pits show a dual slope, which is generally in agreement with experimental data.[15] The

Table 3 Comparison between model predictions and laboratory measurements of plant solutions

Alloy	Model E_{rp}, V vs. SCE		Laboratory Measured E_{rp} @ 95°C V vs. SCE
	95°C	105°C	
Alloy C-276	–0·114	–0·139	–0·138
Alloy AL6XN	–0·257	–0·289	–0·293
Type 316L SS	–0·391	–0·409	–0·544

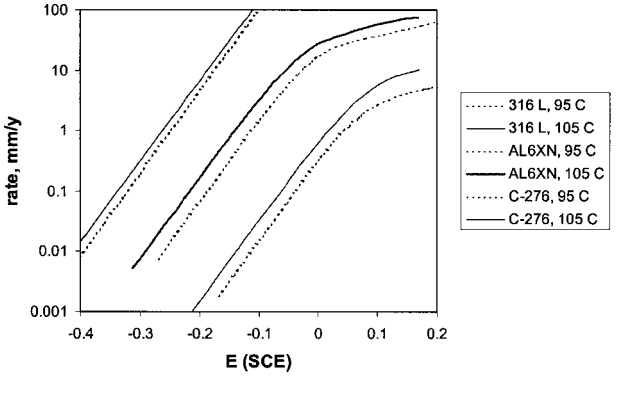

8 Predicted maximum rates of propagation of individual pits as a function of potential at T=95°C (·····) and T=105°C (——) at the conditions of plant tests

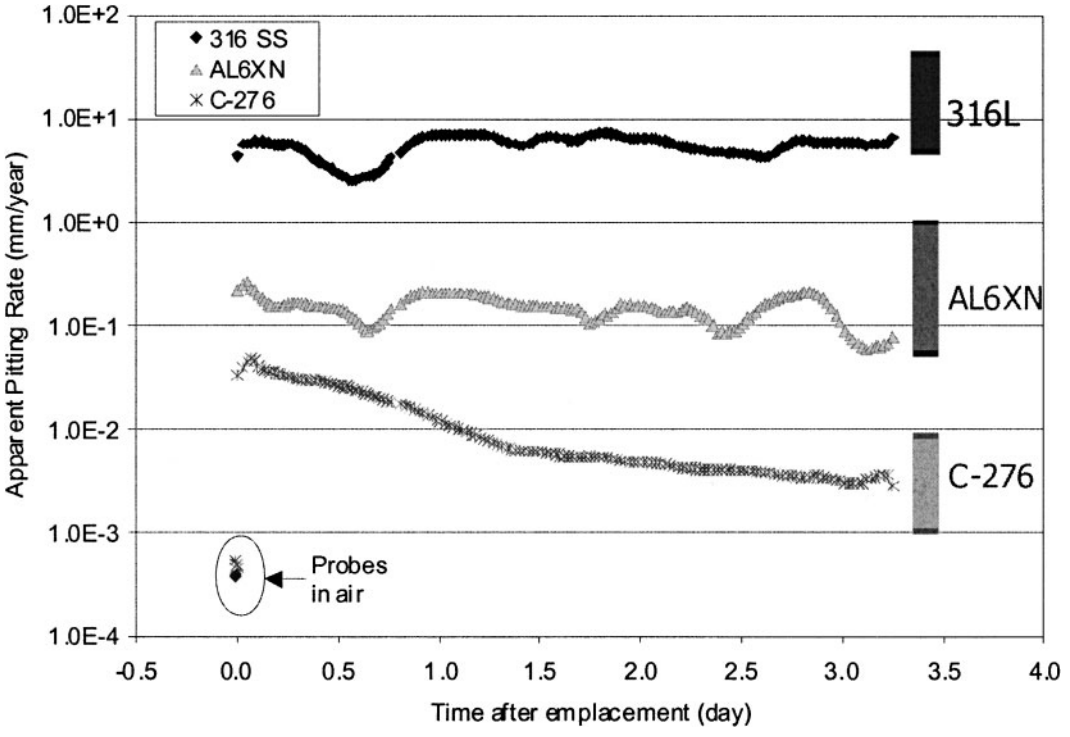

9 Comparison of experimental apparent pitting rates with calculated maximum rates of pit propagation for corrosion potentials obtained from short-term experiments (cf. Fig. 5). The vertical bars show the range of predicted pitting rates when the corrosion potential varies from −0·20 V to −0·14 V (vs SCE) and the temperature varies from 95°C to 105°C

predicted maximum propagation rates can be compared with the observed apparent pitting rates. For this purpose, ranges of propagation rates have been computed for corrosion potentials varying from −0·20 to −0·14 V vs SCE and temperatures varying from 95 to 105°C. The corrosion potential variation from −0·20 to −0·14 V corresponds to the range observed in short term experiments (cf. Fig. 5). It was necessary to make calculations for a certain range of potentials because the predicted propagation rate depends on the potential to a substantial extent. The potential dependence of the propagation rate is illustrated in Fig. 8. Since the model deviates from experimental data at potentials substantially above the repassivation potential, it is expected that the higher propagation rates (above approximately 0·5 mm y^{-1}) are upper estimates rather than accurate predictions.

The predicted propagation rate ranges are compared in Fig. 9 with the apparent pitting rates observed in short-term measurements. The propagation rates were calculated using the nominal area of the electrode. The current density between each electrode and a common junction was measured.[24] The currents differed between electrodes as would be expected for localised corrosion process. The maximum anodic current was used to calculate the propagation rate. In the case of type 316L stainless steel, the effective area of corrosion was smaller than the nominal area. The effective area was used to calculate the corrosion rate. Post-exposure measurement of pit depth through an optical microscope agreed with the electrochemically measured rate. In the case of type 316L stainless steel and alloy AL6XN, the experimentally observed apparent pitting rates are substantial and their values are close to the lower end of the predicted range. Since the model predicts the maximum propagation rates of individual pits, this result demonstrates a very good agreement of the model with the experiment. In the case of alloy C–276, the propagation rates are substantially lower and close to the current at which the repassivation potential is measured (i_{rp}= 10^{-2} A m^{-2}). In this case, the predicted rates should also be close to i_{rp} because the corrosion potential is close to the repassivation potential. This is indeed the case and the predicted range of propagation rates brackets the experimental values. These results provide a stringent test of the proposed methodology and show that the model can be used not only to predict the tendency for localised corrosion, but also to estimate the maximum propagation rate of individual pits.

Conclusions

A localised corrosion model based on repassivation and corrosion potentials has been applied to three Fe–Ni–Cr–Mo–W alloys in a chemical process environment. The three alloys were type 316L stainless steel, alloy AL6XN, and alloy C–276, representing a spectrum of localised corrosion resistance. The process environment consisted of a mixture of chloride, carbonate and hydroxide species along with minor concentrations of oxidising agents arising from the interaction of catalysts and other materials. The model predictions were tested against laboratory data in the process solution as well as data from real time monitoring using multi-electrode array sensor probes installed in the process stream.

1. The predicted repassivation potentials of the alloys in simple chloride solutions agreed reasonably well with measured values for the three alloys.

2. The predicted repassivation potentials for the plant environment agreed well with the repassivation

potentials measured in the laboratory using the solution procured from the plant. The agreement was better for alloys AL6XN and C–276 than for type 316L stainless steel, but the trend in the values was correctly predicted by the model. Because the process fluid data were not used to calibrate the model, the agreement constitutes a stringent test of the model.

3. The measured corrosion potentials were compared to the calculated repassivation potentials in the process stream. The localised corrosion susceptibilities of the three alloys were in agreement with the model predictions based on a comparison of the repassivation and corrosion potentials.

4. As a further step of model validation, the predicted localised corrosion rates were compared to the measured pitting rates in the process stream. Good agreement was obtained between model and measurement.

5. The study also demonstrated the applicability of the multi-electrode array sensor in performing real time monitoring of localised corrosion of chemical process streams.

Acknowledgements

The work reported in this paper was funded by the Advanced Technology Program of the National Institute of Standards and Technology (Cooperative Agreement 70NANB0H3017), and the Department of Energy (Cooperative Agreement DE–FC36–04GO14043) and was co-sponsored by ChevronTexaco, DuPont, ExxonMobil, Mitsubishi Chemical, Rohm&Haas, Shell and Toyo Engineering. The authors also wish to acknowledge the provided by Darrell Dunn, Sean Brossia, Brian Derby, Amanda Smith, and Heather Shore in conducting various supporting experiments, which have been reported elsewhere.

References

1. R. W. STAEHLE, B.F. BROWN, J. KRUGER and A. AGARWAL (eds), U.R. Evans Conf. on 'Localised corrosion', NACE-3, Houston, TX, 1974, NACE International.
2. Z. SZKLARSKA-SMIALOWSKA: 'Pitting corrosion of metals', 1986, NACE International.
3. H.S. ISAACS, U. BERTOCCI, J. KRUGER and S. SMIALOWSKA (eds): 'Advances in localised corrosion, NACE-9', 1990, Houston, TX, NACE International.
4. P. M. NATISHAN, R. G. KELLY, G. S. FRANKEL and R. C. NEWMAN (eds): 'Critical factors in localised corrosion', Vol. 95-15; 1996, Pennington, NJ, The Electrochemical Society.
5. P. M. NATISHAN, H. S. ISAACS, M. JANIK-CZACHOR, V. A. MACAGNO, P. MARCUS and M. SEO (eds): 'Passivity and its breakdown', Vol. 97–26, 1998, Pennington, NJ, The Electrochemical Society.
6. M. SEO, B. MACDOUGALL, H. TAKAHASHI and R.G. KELLY (eds): 'Passivity and its breakdown', 99–27; 1999, Pennington, NJ, The Electrochemical Society.
7. C. Y. CHAO, L. F. LIN and D. D. MACDONALD: *J. Electrochem. Soc.*, 1981, **128**, 1187.
8. L.F. LIN, C.Y. CHAO and D. D. MACDONALD: *J. Electrochem. Soc.*, 1981, **128**, 1194.
9. D. E. WILLIAMS and Y. Y. ZHOU: *J. Electrochem. Soc.*, 2000, **147**, 1763.
10. J. W. OLDFIELD and W. H. SUTTON: *Br. Corros. J.*, 1978, **13**, (1), 13–22.
11. S. M. SHARLAND: Corros. Sci., 1992, **33**, (2), 183–201.
12. S. M. GRAVANO and J. R. GALVELE: *Corros. Sci.*, 1984, **24**, 517–534.
13. M. WATSON and J. POSTLETHWAITE: *Corrosion*, 1990, **46**, 522–530.
14. N. SRIDHAR and D. S. DUNN: *Corrosion*, 1994, **50**, 857.
15. A. ANDERKO, N. SRIDHAR and D. S. DUNN: *Corros. Sci.*, 2004, **46**, 1583–1612.
16. D. S. DUNN, N. SRIDHAR and G. A. CRAGNOLINO: *Corrosion*, 1996, **52**, 115–124.
17. D. S. DUNN, G. A. CRAGNOLINO and N. SRIDHAR: *Corrosion*, 2000, **56**, 90–104.
18. A. ANDERKO and R. D. YOUNG: *Corrosion*, 2000, **56**, 543–555.
19. A. ANDERKO, P. MCKENZIE and R. D. YOUNG: *Corrosion*, 2001, **57**, 202.
20. A. ANDERKO, and M. M. LENCKA. *Ind. Eng. Chem. Res.*, 1998, **37**, 2878–2888.
21. M. M. LENCKA, A. ANDERKO, S. J. SANDERS and R. D. YOUNG: *Int. J. Thermophys.*, 1998, **19**, 367–378.
22. A. ANDERKO, N. SRIDHAR, C.S. BROSSIA, D.S. DUNN, L.T. YANG, B.J. SALDANHA, S.L. GRISE and M. H. DORSEY: Proc. of 'CORROSION 2003', Houston, TX, 2003, NACE International, Paper No. 03375.
23. L. T. YANG, N. SRIDHAR, O. PENSADO and D. S. DUNN: *Corrosion*, 2002, **58**, No. 1004.
24. L. T. YANG and N. SRIDHAR: *Mater. Perform.*, September 2003, 48.
25. D. D. MACDONALD, A. C. SCOTT and P. WENTREEK: *J. Electrochem. Soc.*, 1979, **126**, No. 908.
26. P. WANG, A. ANDERKO and R. D. YOUNG: *Fluid Phase Equilibria*, 2002, **203**, 141–176.
27. B. J. SALDANHA: DuPont Company field corrosion test rack data from 10/2003 to 12/2003. Private Communication, February, 2004.